Which residual mode captures the energy of the dominating mode in second order Hamiltonian systems?

Elvise Berchio[1]   Filippo Gazzola[2]   Chiara Zanini[3]

Abstract

Motivated by the instability of suspension bridges, we consider a class of second order Hamiltonian systems where one component initially holds almost all the energy of the system. We show that if the total energy is sufficiently small then it remains on this component, whereas if the total energy is larger it may transfer to the other components. Through Mathieu equations we explain the precise mechanism which governs the energy transfer.

1   Introduction and motivation

The spectacular collapse of the Tacoma Narrows Bridge (occurred on November 7, 1940, see [2, 20]) raised many questions on the instability of suspension bridges. Soon after the collapse, several theoretical and experimental studies have been performed [6, 7, 15, 18]. The main issue was to understand the origin of the instability [21] and, in particular, how could vertical oscillations be suddenly transformed into destructive torsional oscillations. The focus was essentially on the aerodynamic instability [19] but no conclusive answer was found: in the last few years, the problem of aerodynamic instability of suspension bridges is still under study [9]. Only very recently, the attention has turned to the nonlinear behavior of structures [11].

In [3] and [4] the structural instability of suspension bridges has been highlighted by analyzing two fairly different isolated models. In [3] the bridge was seen as a number of interacting parallel rods representing the cross sections of the bridge, each one having two degrees of freedom: the vertical displacement of the barycenter and the torsional angle. A torsional instability was numerically found: if vertical displacements are sufficiently large then small torsional angles may suddenly grow up leading to the collapse of the bridge. The main tools to reach this result were suitable Poincaré maps [17]. See also [13] for some aerodynamics effects. In [4] the bridge was modeled as a degenerate plate, named fish-bone by the authors, where the midline of the plate was seen as a beam and virtual orthogonal cross sections were considered free to rotate about their center placed on the beam. See also [5] where the aerodynamic forces were introduced in the model. The same torsional instability was found, both numerically and theoretically, and the instability was justified through the analysis of suitable Hill equations [10].

[1]Department of Mathematical Sciences, Politecnico di Torino, Corso Duca degli Abruzzi 24, 10129 Torino, Italy, E-Mail: `elvise.berchio@polito.it`

[2]Department of Mathematics, Politecnico di Milano, Piazza Leonardo da Vinci 32, 20133 Milano, Italy, E-Mail: `filippo.gazzola@polimi.it`

[3]Department of Mathematical Sciences, Politecnico di Torino, Corso Duca degli Abruzzi 24, 10129 Torino, Italy, E-Mail: `chiara.zanini@polito.it`

It is clear that there is a relation between these two models and approaches. This is probably due to the connection between Poincaré and Hill, as testified in [16]; their work takes the origin from celestial mechanics and, as we just saw, it applies as well to suspension bridges. The results in [3, 4] lead to the very same conclusion: if vertical oscillations are small enough then small initial torsional oscillations remain small for all the time, whereas if vertical oscillations are large then small torsional oscillations can suddenly become wider. This gives an answer to a long-standing question raised by the Tacoma Narrows Bridge collapse, see [2, 20], namely how can destructive torsional oscillations suddenly appear in a vertically oscillating bridge. The main core in both [3, 4] is the stability analysis of vertical modes, that is, how can a bridge oscillating as an almost pure vertical mode suddenly transfer part of the energy to a torsional mode. We investigate this phenomenon by considering a class of second order Hamiltonian systems such as

$$\ddot{y}_i + \lambda_i^2 y_i + U_{y_i}(Y) = 0, \qquad Y = (y_1, \ldots, y_n) \in \mathbb{R}^n \tag{1.1}$$

for some $n \geq 2$, $\lambda_i > 0$ and some potential $U \in C^1(\mathbb{R}^n, \mathbb{R})$, where U_{y_i} denotes the partial derivative of U with respect to y_i. The heart of the matter is to study the evolution of the solutions of (1.1) satisfying the initial conditions

$$y_1(0) = \zeta_0, \ \dot{y}_1(0) = \zeta_1, \qquad \sum_{i=2}^{n}(|y_i(0)| + |\dot{y}_i(0)|) \ll |\zeta_0| + |\zeta_1| \tag{1.2}$$

for $\zeta_0, \zeta_1 \in \mathbb{R}$; due to these uneven boundary conditions, we call y_1 the *dominating mode* and y_i (for $i = 2, ..., n$) the *residual modes*. And the main question is to establish if the unique solution $Y = Y(t)$ of (1.1)-(1.2) has small residual modes for every time $t > 0$. It was shown in [3, 4] that this is true provided that $|\zeta_0| + |\zeta_1|$ is sufficiently small whereas it may become false if $|\zeta_0| + |\zeta_1|$ is sufficiently large. The typical pictures describing the instability of (1.1)-(1.2) are as in Figure 1.
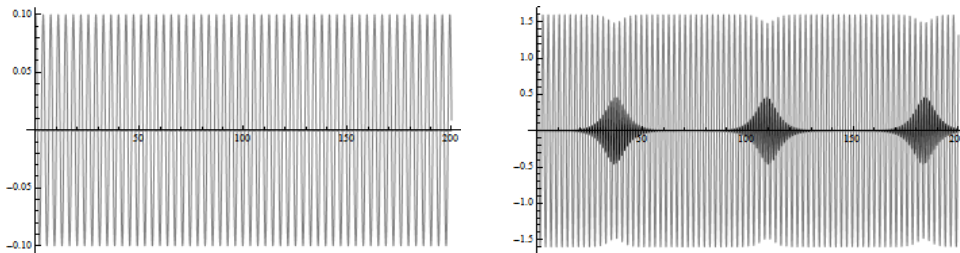

Figure 1: Stable and unstable oscillations.

In both pictures, the gray oscillations represent the dominating mode whereas the black oscillations represent the largest component among the residual modes. In the left picture, the initial data ζ_0 and ζ_1 in (1.2) are small and the only large component of Y is y_1 for all $t > 0$, no black oscillations are visible. In the right picture, the initial data ζ_0 and ζ_1 in (1.2) are larger and one may see a large oscillation also in one of the residual modes: this mode suddenly grows up by capturing some energy from y_1 which decreases its amplitude of oscillation when the transfer of energy occurs. This is what we call instability of y_1 (for large energies) and it can be seen for many different forms of the potential U in (1.1), see [3].

A question was left open in [3, 4]: which residual mode first captures the energy of y_1? Moreover, which is the criterion governing the transfer of energy? The relevance of these questions relies on the possibility to understand which kind of oscillating mode will first appear in the bridge when enough energy is inside the structure. In particular, this could help to prevent the appearance of the destructive torsional oscillations. The main purpose of this paper is to give a sound answer to these questions.

We consider a simple prototype problem like (1.1)-(1.2) with $n = 3$. We choose a potential U in such a way that the linearized problem becomes a system of Mathieu equations [12], which are a particular case

of the Hill equations. The advantage of this choice is that much more precise information is known on the behavior of the stability regions. Exploiting this fact we give a detailed explanation of how the stability is lost for the dominating mode of (1.1) and which residual mode first captures its energy. Notice that by [3] we know that several different choices of U yield a similar response in the bridge.

The paper is organized as follows. In Section 2 we state the theoretical criterion governing the energy transfer between modes and in Section 3 we collect several numerical experiments which confirm and illustrate the theoretical results. In Section 4 we discuss different choices of the potential U. Finally, in Section 5 we give a mechanical interpretation of the numerical results and we suggest some structural remedies to prevent instability in suspension bridges.

2 Main results: energy dependent stability

For μ, λ_1, λ_2 being positive real numbers, $x_0 \in \mathbb{R} \setminus \{0\}$ and $\varepsilon > 0$, we consider the following problem

$$\begin{cases} \ddot{y} + \mu^2 y + U_y(y, z_1, z_2) = 0 & y(0) = x_0, \ \dot{y}(0) = 0 \\ \ddot{z}_1 + \lambda_1^2 z_1 + U_{z_1}(y, z_1, z_2) = 0 & z_1(0) = \varepsilon x_0, \ \dot{z}_1(0) = 0 \\ \ddot{z}_2 + \lambda_2^2 z_2 + U_{z_2}(y, z_1, z_2) = 0 & z_2(0) = \varepsilon x_0, \ \dot{z}_2(0) = 0, \end{cases} \tag{2.1}$$

where $U : \mathbb{R}^3 \to \mathbb{R}$ is a non-negative, differentiable function with locally Lipschitz derivatives, and U_y, U_{z_i} stand for its partial derivatives with respect to y and z_i, respectively. The conserved total energy of (2.1) is given by

$$E := \frac{\dot{y}^2}{2} + \frac{\dot{z}_1^2}{2} + \frac{\dot{z}_2^2}{2} + \frac{\mu^2}{2}y^2 + \frac{\lambda_1^2}{2}z_1^2 + \frac{\lambda_2^2}{2}z_2^2 + U(y, z_1, z_2). \tag{2.2}$$

Along the paper, we mainly deal with the potential

$$U(y, z_1, z_2) = \frac{y^2 z_1^2 + y^2 z_2^2 + z_1^2 z_2^2}{2}, \tag{2.3}$$

see Section 4 for a discussion about different choices. With the potential U as in (2.3), system (2.1) becomes

$$\begin{cases} \ddot{y} + \mu^2 y + (z_1^2 + z_2^2)y = 0 & y(0) = x_0, \ \dot{y}(0) = 0 \\ \ddot{z}_1 + \lambda_1^2 z_1 + (y^2 + z_2^2)z_1 = 0 & z_1(0) = \varepsilon x_0, \ \dot{z}_1(0) = 0 \\ \ddot{z}_2 + \lambda_2^2 z_2 + (y^2 + z_1^2)z_2 = 0 & z_2(0) = \varepsilon x_0, \ \dot{z}_2(0) = 0. \end{cases} \tag{2.4}$$

If in (2.4) we take $\varepsilon = 0$ (and $x_0 \neq 0$), then its unique solution satisfies $z_1 \equiv z_2 \equiv 0$, while y solves $\ddot{y} + \mu^2 y = 0$. Notice that, up to a time translation, any initial condition $(y(0), \dot{y}(0)) \neq (0,0)$, yields the same solution as $(y(0), \dot{y}(0)) = (x_0, 0)$ for some x_0. Therefore, for $\varepsilon = 0$ (and $x_0 \neq 0$), system (2.4) admits the unique solution $(\bar{y}, 0, 0) = (x_0 \cos(\mu t), 0, 0)$ and the conserved energy

$$E := \frac{\dot{y}^2}{2} + \frac{\mu^2}{2}y^2 = \frac{\mu^2}{2}x_0^2. \tag{2.5}$$

Since our aim is to study the behavior of solutions for small ε, we linearize the z_i equations of (2.4) around this solution and we obtain the following system of Mathieu equations [14]

$$\begin{cases} \ddot{\xi}_1 + \left(\lambda_1^2 + \frac{x_0^2}{2} + \frac{x_0^2}{2}\cos(2\mu t)\right)\xi_1 = 0 \\ \ddot{\xi}_2 + \left(\lambda_2^2 + \frac{x_0^2}{2} + \frac{x_0^2}{2}\cos(2\mu t)\right)\xi_2 = 0. \end{cases} \tag{2.6}$$

By a change of variables (without renaming the ξ_i's), we may rewrite the equations in (2.6) in the canonical form:

$$\ddot{\xi}_i + (\alpha_i + 2q_i \cos(2t))\xi_i = 0, \quad \text{for } i = 1, 2, \tag{2.7}$$

3

with

$$\alpha_i(x_0) = \frac{2\lambda_i^2 + x_0^2}{2\mu^2} \quad \text{and} \quad q_i(x_0) = q(x_0) = \frac{x_0^2}{4\mu^2} \quad \text{for } i = 1, 2 \,, \tag{2.8}$$

so that

$$\alpha_i(q) = \frac{\lambda_i^2}{\mu^2} + 2q \,. \tag{2.9}$$

Let us explain what we mean by stability for system (2.4).

Definition 2.1. *The solution* $(\bar{y}, 0, 0) = (x_0 \cos(\mu t), 0, 0)$ *to system* (2.4) *for* $\varepsilon = 0$ *is said to be stable if the trivial solutions* $\xi_i \equiv 0$ *(i = 1, 2) of* (2.7) *are both stable. In the other cases,* $(\bar{y}, 0, 0)$ *is said to be unstable.*

Note that the two equations in (2.7) are uncoupled and therefore the trivial solution $(\xi_1, \xi_2) = (0, 0)$ is stable if and only if both the trivial solutions $\xi_1 = 0$ and $\xi_2 = 0$ of each equation in (2.7) are stable. The numerical results described in Section 3 confirm that this definition is well suited to characterize the instability. As we shall see, the stability of $(\bar{y}, 0, 0)$ depends on its energy (2.5). Therefore, the following definition will be useful.

Definition 2.2. *We say that the energy* E *in* (2.5) *is activating for the residual mode* z_i *(i = 1 or i = 2) of system* (2.4) *if the trivial solution* $\xi_i \equiv 0$ *of the Mathieu equation* (2.7) *is unstable. Otherwise, we say that it is non-activating.*

We may now state and prove the following stability result.

Theorem 2.3. *Let* $\mu, \lambda_1, \lambda_2 > 0$ *and* $x_0 \in \mathbb{R} \setminus \{0\}$. *Let* $E > 0$ *be the energy* (2.5) *associated to the solution* $(\bar{y}, 0, 0) = (x_0 \cos(\mu t), 0, 0)$ *to system* (2.4) *for* $\varepsilon = 0$. *For each* $i = 1, 2$ *there exists an increasing divergent sequence* $\{E_m^i\}_{m=0}^\infty$ *such that* $E_0^i = 0$ *and*
  (i) E *is non-activating whenever* $E \in (E_{2k}^i, E_{2k+1}^i)$ *for some* $k \geq 0$;
  (ii) E *is activating whenever* $E \in (E_{2k+1}^i, E_{2k+2}^i)$ *for some* $k \geq 0$.

Proof. We first recall that, given $q > 0$, the Mathieu equation

$$\ddot{w} + (a + 2q \cos(2t)) \, w = 0$$

admits solutions which are either π or 2π-periodic only if a belongs to the countably infinite sets of the so-called Mathieu characteristic values $\{a_n(q)\}_{n \geq 0}$ and $\{b_n(q)\}_{n \geq 1}$, see [1, 14, 22]. The characteristic curves do not intersect, that is, we have

$$a_0(q) < b_1(q) < a_1(q) < \cdots < b_n(q) < a_n(q) < b_{n+1}(q) < \ldots \qquad \forall n \geq 2 \,. \tag{2.10}$$

Moreover, their asymptotic behavior for large q is

$$a_n(q) \sim -2q \,, \quad b_n(q) \sim -2q \qquad \text{as } q \to \infty \,, \tag{2.11}$$

while for small q we have

$$\begin{cases} a_0(q) = o(q) \,, \quad b_1(q) = 1 - q + o(q) \,, \quad a_1(q) = 1 + q + o(q) \,, \\ b_n(q) = n^2 + o(q) \quad \text{and} \quad a_n(q) = n^2 + o(q) \quad \forall n \geq 2 \,, \end{cases} \qquad \text{as } q \to 0 \,, \tag{2.12}$$

see [14, Sections 2.151 and 12.30].

The characteristic curves $a_n(q)$ and $b_n(q)$ divide the (q, a)-plane into stable and unstable regions, see the left picture in Figure 2, where the red lines correspond to the characteristic curves. Denote with S_n ($n \geq 0$) the stability (white) regions and with U_n ($n \geq 1$) the instability (gray) regions. For $n \geq 0$ we have

$$S_n := \{(q, a) : q > 0 \,, a_n(q) < a < b_{n+1}(q)\},$$

while for $n \geq 1$ we have
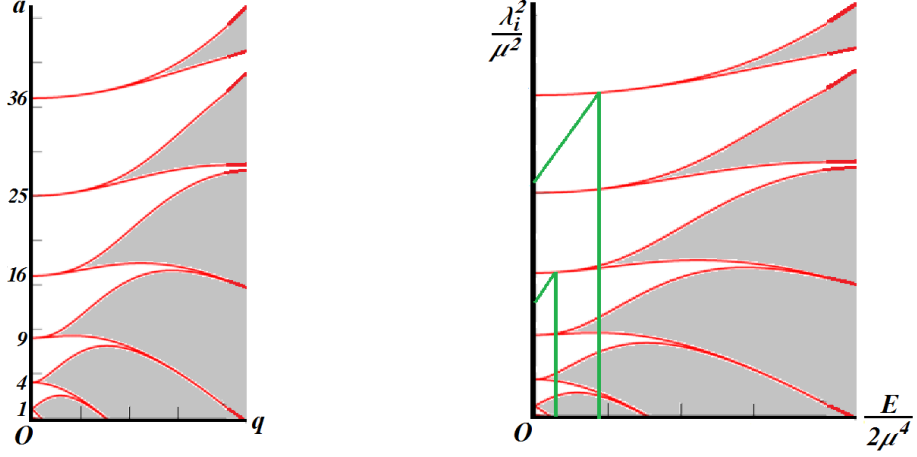
$$U_n := \{(q,a) : q > 0, b_n(q) < a < a_n(q)\}.$$

Figure 2: On the left the Mathieu diagram, on the right how to compute the energy threshold. The instability regions are gray.

To each couple (μ, λ_i) in system (2.4) we associate the sequence of energies $\{E_m^i\}_{m=0}^\infty$ as follows. The energy associated to $(\bar{y}, 0, 0)$ satisfies (2.5), that is

$$E = \frac{\mu^2 x_0^2}{2} = 2\mu^4 q, \qquad (2.13)$$

where the second equality is due to (2.8). Hence, as E increases from $E = 0$ to $E = \infty$ the parameters $(q(x_0), \alpha_i(x_0))$ in (2.7) move along the line (2.9) in the (q,a)-plane, according to the law (2.8). We need to study the intersections of these lines with S_n and U_n.

If $\alpha_i(0) = \lambda_i^2/\mu^2 \in (n^2, (n+1)^2) \equiv (a_n(0), b_{n+1}(0))$ for some $n = 0, 1, 2, \dots$ then, since all the functions involved are continuous, there exists $E_1^i > 0$ such that $a_n(q) < \alpha_i(q) < b_{n+1}(q)$ for all $E < E_1^i$, that is, for all $q > 0$ sufficiently small in view of (2.13). If $\alpha_i(0) = \lambda_i^2/\mu^2 = n^2 = a_n(0) < (n+1)^2 = b_{n+1}(0)$ for some $n = 1, 2, \dots$ then, since the lines (2.9) have slope 2 and since (2.12) holds, we conclude again that $a_n(q) < \alpha_i(q) < b_{n+1}(q)$ for all $E > 0$ sufficiently small. Therefore,

$$\exists n \in \mathbb{N}, \quad \exists E_1^i > 0 \text{ s.t. } (q, \alpha_i(q)) \in S_n \qquad \forall E < E_1^i. \qquad (2.14)$$

The largest possible value of E_1^i may be determined as follows: one finds the abscissa q of the intersection between $\alpha_i(q)$ and $b_{n+1}(q)$ where n is as in (2.14) (see the corner of the green line in the right picture of Figure 2), then one computes E_1^i according to (2.13). The asymptotic estimate (2.11) ensures that $E_1^i < \infty$.

By (2.10)-(2.11)-(2.12) we infer that the straight line (2.9) intersects at least once each characteristic curve a_n and b_n provided that $n > \lambda_i/\mu$; moreover, at each crossing, the line moves from some U_n to S_n or from some S_n to U_{n+1}, thereby alternating its intersection with gray and white regions in Figure 2. Since the stability of the trivial solution $\xi_i \equiv 0$ of (2.7) depends on the position of (q, α_i) in the Mathieu diagram, this completes the proof of the theorem. $\qquad \square$

Theorem 2.3 states, in particular, that the first energy interval $(0, E_1^i)$ is non-activating for both $i = 1, 2$. We may rephrase this property as follows.

5

Corollary 2.4. *For every triple of real positive parameters $(\mu, \lambda_1, \lambda_2)$ there exists an energy $\bar{E} = \bar{E}(\mu, \lambda_1, \lambda_2) > 0$ such that the solution $(\bar{y}, 0, 0)$ to system (2.4) for $\varepsilon = 0$ is stable provided that its conserved energy E defined in (2.5) satisfies $E \leq \bar{E}$.*

By combining Theorem 2.3 with Definition 2.2 we obtain the following theoretical criterion to determine which residual mode captures the energy of the dominating mode y:

Corollary 2.5. *Let $E > 0$ be the energy (2.5) of system (2.4) associated to the solution $(\bar{y}, 0, 0)$ for $\varepsilon = 0$. If $E \in (E_{2k+1}^i, E_{2k+2}^i)$ for some $k \geq 0$ and for $i = 1$ or $i = 2$, then the residual mode z_i captures the energy of the dominating mode y.*

As we shall see in Section 3 it may happen that both the residual modes capture the energy. Furthermore, the amount of captured energy depends on how far is the point (q, a) from the stability region. Therefore, the amplitude of the corresponding activating interval plays an important role. In Section 3 we shall see that if it is sufficiently small then there is no "visible" activation, since the crossing through the unstable region is "too fast".

3 Numerical results

We consider again system (2.4). For ε small, its conserved energy is given by

$$E = \frac{1}{2}\left(\dot{y}^2 + \dot{z_1}^2 + \dot{z_2}^2 + \mu^2 y^2 + \lambda_1^2 z_1^2 + \lambda_2^2 z_2^2 + y^2 z_1^2 + y^2 z_2^2 + z_1^2 z_2^2\right) \approx \frac{\mu^2}{2}\, x_0^2 . \tag{3.1}$$

From the proof of Theorem 2.3 we learn that the activating intervals for the energy can be computed by determining for which values of q the couple (q, α_i) in (2.8) lies in the instability regions U_n with $n^2 > \alpha_i(0)$, namely by intersecting the lines (2.9) with the characteristic curves of the Mathieu equations. A numerical approximation of the intersection points can be obtained with Mathematica, by using the functions

<div align="center">

`MathieuCharacteristicA[n,x]` and `MathieuCharacteristicB[n,x]` .

</div>

In turn, by (2.8), this intersection yields the initial data x_0 for which the energy belongs to the activating intervals. In the experiments below we plot the solutions to (2.4) for suitable choices of the parameters $\mu, \lambda_1, \lambda_2$ and for different values of the initial data x_0.

3.1 Experiment 1

Fix $\mu^2 = 1$, $\lambda_1^2 = 0.1$, $\lambda_2^2 = 0.9$ and $\varepsilon = 10^{-3}$. By computing, as explained above, the intersection points of the characteristic curves of the Mathieu equations $b_1 < a_1 < b_2 < a_2$ with the straight lines:

$$(\ell_1) \quad a = 0.1 + 2q \qquad \text{and} \qquad (\ell_2) \quad a = 0.9 + 2q \tag{3.2}$$

and thanks to (2.8), we obtain that the couple $(q, \alpha_1(q))$, as given in (2.9), lies in the instability region U_1 (resp. U_2) if x_0 belongs to the interval $I_1^1 = (1.1, 1.8)$ (resp. $I_1^2 = (2.69, 3.44)$). For these choices of x_0 the energy (3.1) is activating for z_1. Similarly, if x_0 belongs to the interval $I_2^1 = (0.36, 0.63)$ (resp. $I_2^2 = (2.42, 2.99)$), then the couple $(q, \alpha_2(q))$ lies in the instability region U_1 (resp. U_2) and the corresponding energy (3.1) is activating for z_2.

With Mathematica we plot the graphs of the solution of (2.4) on the interval of time $t \in [0, 400]$ for varying x_0 (and, therefore, varying E) close to the intervals determined above. We varied x_0 from $x_0 = 0.1$ to $x_0 = 3$ with step 0.1; we obtained plots of the residual modes z_1 and z_2 and we could see which of the two modes (if any) captured the energy of the dominating mode y. We also plotted the

graph of y which is somehow less interesting since for small $t > 0$ it essentially looks like $y(t) \approx x_0 \cos(\mu t)$ and is too large to allow to see the variations of the residual modes z_i. Since both the z_i start with amplitude of oscillations of the order of 10^{-3} (or even 10^{-4} for small x_0), we could detect their instability when their oscillations increased in amplitude of at least one order of magnitude. In order not to plot too many pictures, we describe the obtained results with 15 graphs from $x_0 = 0.2$ to $x_0 = 3$ with step 0.2. All the graphs are complemented with comments.
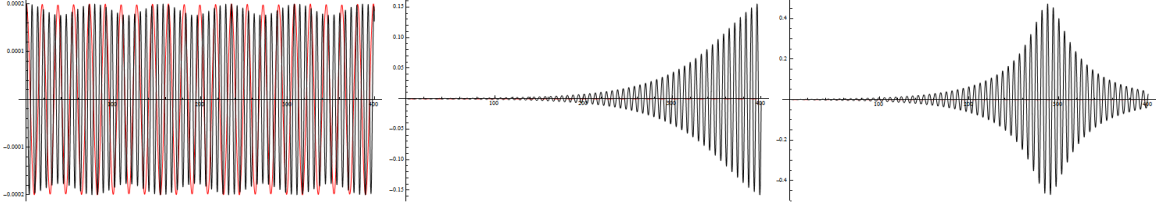

Figure 3: Plots of z_1 (red) and z_2 (black) for $x_0 \in \{0.2, 0.4, 0.6\}$ (left to right).

In Figure 3 we display the plots for $x_0 \in \{0.2, 0.4, 0.6\}$. It is apparent that for $x_0 = 0.2$ both the residual modes remain small, nearly as their initial amplitude. It is however already visible that z_2 (black) has somehow regular cycles of variable amplitude. For $x_0 = 0.4$ we only see z_2 which grows up to $\approx 0.16 \gg z_2(0)$ while z_1 is not visible because it remains of the order of $z_1(0)$; this picture shows that z_2 has captured some of the energy of y whose amplitude has decreased as in Figure 1. The same phenomenon is accentuated for $x_0 = 0.6$ where it appears earlier in time and z_2 grows up until ≈ 0.43.

Let us analyze these results with the aid of the theoretical results of Section 2. We enlarge the diagram of the instability curves of the Mathieu equations and, on the same graph, we plot the straight lines ℓ_1 and ℓ_2 as defined in (3.2). Since we are in the region where $a \leq 1$, the obtained picture on the interval $q \in [0, 1/4]$ is represented in Figure 4.
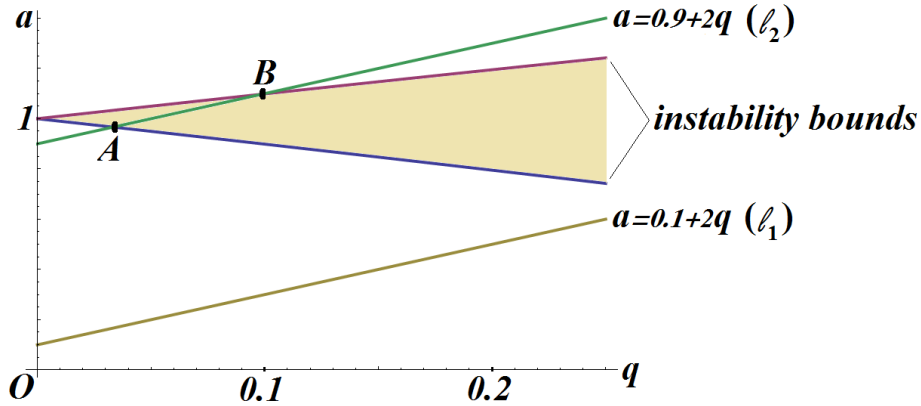

Figure 4: Intersections between the stability regions and the parametric lines (local view).

Starting from $q = 0$ (that is, $x_0 = 0$), the line (ℓ_2) is the first one which exits the (white) stability region. This happens at the point A which, again computed with Mathematica, has the abscissa $q \approx 0.033$ and therefore, in view of (2.8), $x_0 \approx 0.36$, i.e. the left endpoint of the interval I_2^1. At this amplitude of oscillation of y, in accordance with our theoretical results, we see that the residual mode z_2 starts capturing its energy. Figure 3 confirms that the transition occurs for $0.2 < x_0 < 0.4$. In view of (3.1), the critical energy is $E \approx 0.066$.

For larger x_0, that is $x_0 \in \{0.8, 1, 1.2\}$, we obtained the plots in Figure 5. In the first two pictures
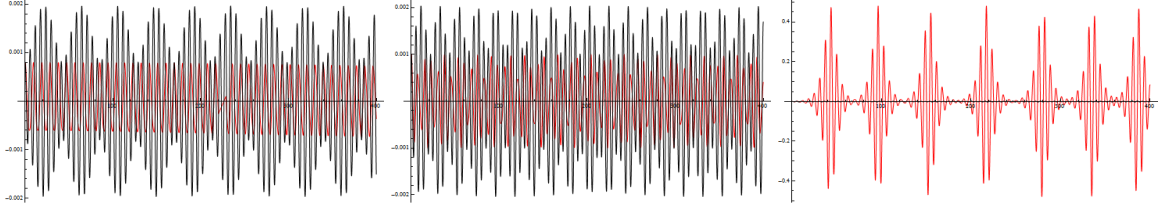
Figure 5: Plots of z_1 (red) and z_2 (black) for $x_0 \in \{0.8, 1, 1.2\}$ (left to right).

($x_0 \in \{0.8, 1\}$) we see that none between z_1 and z_2 captures the energy of y, they essentially remain of the same order of magnitude as the initial data. This means that the line (ℓ_1) has not yet entered in the instability region of the Mathieu diagram while (ℓ_2) has exited. Looking again at Figure 4, we see that the latter fact occurs at the point B corresponding to $q \approx 0.099$ and therefore to $x_0 \approx 0.63$, i.e. the right endpoint of the interval I_2^1. At this amplitude of oscillation of y, the residual mode z_2 stops capturing its energy. Figures 3 and 5 confirm that the transition occurs for $0.6 < x_0 < 0.8$. Namely, the activating interval numerically observed is the one determined by the theoretical results. Moreover, Figure 4 also shows that (ℓ_1) has not yet entered in the instability region: in order to see when this happens we have to take a larger view of the Mathieu diagram, see Figure 6. In this picture we represent the diagram for
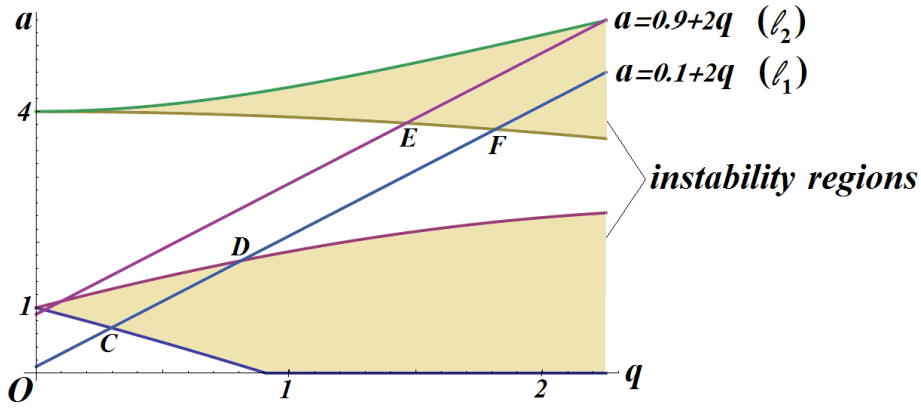

Figure 6: Intersections between the stability regions and the parametric lines (global view).

$q \in [0, 9/4]$ since $q = 9/4$ corresponds to $x_0 = 3$; moreover, we do not place again the points A and B in order to have a more readable picture. The point where (ℓ_1) enters the instability region is C, see Figure 6: numerically, it corresponds to $q \approx 0.3$ and to $x_0 \approx 1.1$ (left endpoint of I_1^1). This explains why in Figure 5, case $x_0 = 1.2$, we see that z_1 enlarges and captures the energy of the dominating mode y.

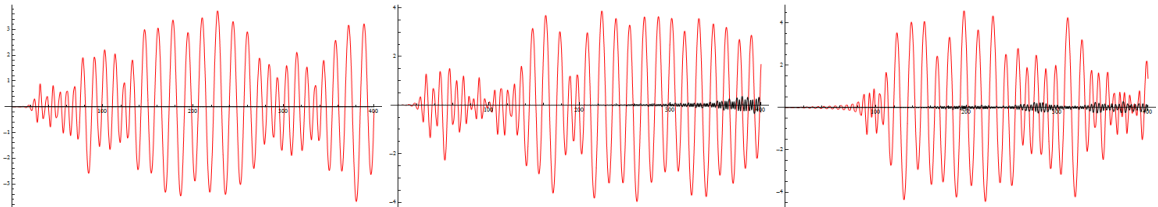By increasing further x_0, that is, $x_0 \in \{1.4, 1.6, 1.8\}$ we obtained the plots in Figure 7.

Figure 7: Plots of z_1 (red) and z_2 (black) for $x_0 \in \{1.4, 1.6, 1.8\}$ (left to right).

We see here that z_1 may become even larger than x_0, that is, of the initial amplitude of the dominating mode. From the energy conservation we infer that this can happen only if y is almost 0 when $|z_1|$ reaches its maximum. This shows that there has been a change of the frequencies and that the period of z_1 is a multiple (possibly the same) of the period of y. For $x_0 \in \{1.6, 1.8\}$ we see that also z_2 increases its amplitude after some (long) interval of time. We believe that this happens because z_2 captures some energy from z_1; this would mean that the linearized problem has changed and that different straight lines should be drawn on the Mathieu diagram. Therefore, this *does not* mean that (ℓ_2) has reached the point E in Figure 6.

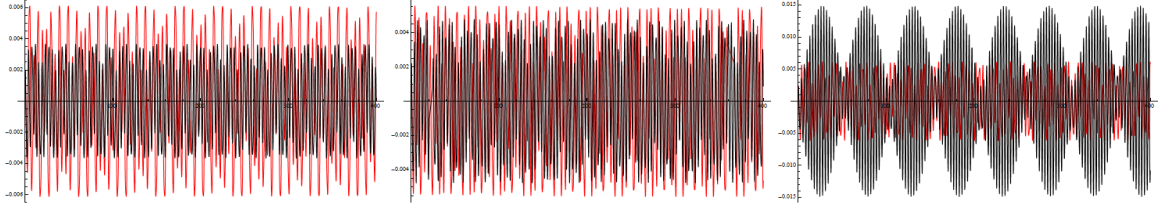For $x_0 \in \{2, 2.2, 2.4\}$ we obtained the plots in Figure 8.

Figure 8: Plots of z_1 (red) and z_2 (black) for $x_0 \in \{2, 2.2, 2.4\}$ (left to right).

If $x_0 \in \{2, 2.2\}$ we see that no residual mode is capturing the energy of the dominating mode, both z_1 and z_2 have an amplitude of oscillation of the order of 10^{-3}. This means that the line (ℓ_1) has crossed the point D which, numerically, is seen to occur for $q \approx 0.81$ and to $x_0 \approx 1.8$ (right endpoint of I_1^1). This fact is confirmed by a finer experiment performed for $x_0 = 1.81$: in this case, the picture looks like the left one in Figure 8. If $x_0 = 2.4$, from Figure 8 we see that z_2 starts to become larger, which means that the line (ℓ_2) is approaching the point E in Figure 6. And, indeed, we numerically found that the abscissa of E is $q \approx 1.46$ which corresponds to $x_0 \approx 2.42$ (left endpoint of I_2^2).

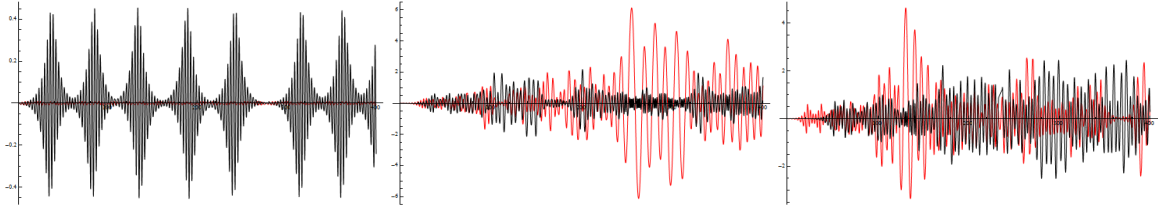For $x_0 \in \{2.6, 2.8, 3\}$ we obtained the plots in Figure 9.

Figure 9: Plots of z_1 (red) and z_2 (black) for $x_0 \in \{2.6, 2.8, 3\}$ (left to right).

For $x_0 = 2.6$ the line (ℓ_2) is beyond E and has entered in the second instability region, a fact which is clearly displayed by the left picture in Figure 9. The point F in Figure 6 is the point where also (ℓ_1) enters in the second instability region: its abscissa is $q = 1.81$ corresponding to $x_0 \approx 2.69$ (left endpoint of I_1^2). And indeed, the plots for $x_0 \in \{2.8, 3\}$ essentially show a chaotic behavior where both the residual modes capture the energy of the dominating mode.

The just described numerical results enable us to give a precise answer to the question raised in the title relatively to the particular second order Hamiltonian system (2.4).

> *Which residual mode captures the energy of the dominating mode depends on the amplitude of oscillation or, equivalently, on the amount of energy present within (2.4).*

The response is summarized in the following table where RMCE means *residual mode capturing the energy* and x_0 varies in the interval $[0, 3]$.

Table 1: residual mode capturing the energy (RMCE) when $\mu^2 = 1$, $\lambda_1^2 = 0.9$ and $\lambda_2^2 = 0.1$.

$x_0 \in$	$[0, 0.36)$	I_2^1	$(0.63, 1.1)$	I_1^1	$(1.8, 2.42)$	$I_2^2 \setminus I_1^2$	$I_2^2 \cap I_1^2$
RMCE	none	z_2	none	z_1	none	z_2	both

3.2 Experiment 2

Consider system (2.4) with $\mu = 1$, $\lambda_1 = 2$, $\lambda_2 = 4$ and $\varepsilon = 10^{-3}$. We proceed as in Experiment 1. The straight lines (2.9) in this case are

$$(\ell_1) \quad a = 4 + 2q \qquad \text{and} \qquad (\ell_2) \quad a = 16 + 2q.$$

To determine the first two activating intervals for each of the residual modes, we first intersect ℓ_1 with the characteristic curves $b_3 < a_3 < b_4 < a_4$ and then ℓ_2 with the characteristic curves $b_5 < a_5 < b_6 < a_6$. With Mathematica and recalling (2.8), we obtain that the couple $(q, \alpha_1(q)) = (q, 4 + 2q)$ lies in the instability region U_3 (resp. U_4) if x_0 belongs to the interval $I_1^1 = (3.22, 3.42)$ (resp. $I_1^2 = (5.08, 5.42)$). For these choices of x_0 the energy (3.1) is activating for z_1. The couple $(q, \alpha_2(q)) = (q, 16 + 2q)$ lies in the instability region U_5 (resp. U_6) if x_0 belongs to the interval $I_2^1 = (4.349, 4.357)$ (resp. $I_2^2 = (6.58, 6.614)$) and the energy (3.1) is activating for z_2. As in Section 3.1, we have plotted the graphs of z_1 and z_2 for many choices of x_0 both inside and outside the above intervals I_i^j. For x_0 entering in the intervals I_1^1 and I_1^2, the behavior of the solutions z_1 and z_2 is as in Figure 3 with z_1 and z_2 swapped. The amplitude of the oscillations of z_1 increases by a factor of 10 when crossing I_1^1 and by a factor of 4 when crossing I_1^2. If x_0 belongs to I_2^1 the energy transfer on z_2 cannot be noticed. The reason is the small amplitude of the interval I_2^1 (of order $< 10^{-2}$); in other words, for small energies z_2 appears more stable than z_1. Finally, if x_0 belongs to the interval I_2^2 the energy transfer on z_2 can hardly be noticed, since the amplitude of the oscillations of z_2 increases by a factor of 2 when crossing I_2^2. The results are summarized in Table 2.

Table 2: residual mode capturing the energy (RMCE) when $\mu^2 = 1$, $\lambda_1^2 = 4$ and $\lambda_2^2 = 16$.

$x_0 \in$	$[0, 3.22)$	I_1^1	$(3.42, 4.349)$	I_2^1	$(4.357, 5.08)$	I_1^2	$(5.42, 6.58)$	I_2^2
RMCE	none	z_1	none	none	none	z_1	none	z_2/none

3.3 Experiment 3

We fix $\mu = \sqrt{2}/2$, $\lambda_1 = 2$, $\lambda_2 = 4$ and $\varepsilon = 10^{-2}$, namely we double the ratios $\frac{\lambda_i^2}{\mu^2}$ of Experiment 2. Here the straight lines (2.9) become

$$(\ell_1) \quad a = 8 + 2q \qquad \text{and} \qquad (\ell_2) \quad a = 32 + 2q.$$

With Mathematica, we intersect ℓ_1 with the characteristic curves $b_3 < a_3 < b_4 < a_4$ and ℓ_2 with the characteristic curves $b_6 < a_6 < b_7 < a_7$. By (2.8), arguing as in the previous experiments, we obtain that if x_0 belongs to the intervals $I_1^1 = (1.007, 1.009)$ and $I_1^2 = (2.915, 2.969)$, then the energy (3.1) is activating for z_1. If x_0 belongs to the intervals $I_2^1 = (2.01467, 2.01468)$ and $I_2^2 = (4.2233, 4.2239)$, then the energy (3.1) is activating for z_2. The behavior of both z_1 and z_2 becomes much more stable and we have to wait until the second activating interval for z_1, namely I_1^2, to register the first significant energy transfer on a residual mode. Table 3 summarizes what we numerically observed.

Table 3: Residual mode capturing the energy (RMCE) when $\mu^2 = 1/2$, $\lambda_1^2 = 4$ and $\lambda_2^2 = 16$.

$x_0 \in$	$[0, 1.007)$	I_1^1	$(1.009, 2.01467)$	I_2^1	$(2.01468, 2.915)$	I_1^2	$(2.969, 4.2233)$	I_2^2
RMCE	none	none	none	none	none	z_1	none	none

3.4   Conclusions from the numerical results

We performed further experiments which confirmed the just illustrated precise pattern. The lines (2.9) intersect alternatively the stability/instability regions giving rise to one of the above pictures. Furthermore, the observed activating intervals coincide with those expected from our theoretical results. Summarizing, we may draw the following conclusions.

• Which residual mode first captures the energy of the dominating mode depends on the *ratios* λ_i/μ: these ratios determine the point of the a-axis in the Mathieu diagram where the straight lines (2.8) start at zero energy.

• The energy threshold for instability is $\mu^2 x_0^2/2$, see (2.13), and one can use Figure 2 to compute it.

• The residual modes grow up earlier in time and wider in amplitude if x_0 is such that the corresponding parameters (q, α_i) in (2.8) are far from the stability region, see the last two pictures in Figure 3.

• When the quotient $\frac{\lambda_i^2}{\mu^2}$ increases, the residual modes display a very stable behavior. A theoretical explanation of this fact comes from the classical stability theory for the Mathieu equation. Indeed, it can be proved that for $a \gg q > 0$, corresponding in our case to $\frac{\lambda_i^2}{\mu^2}$ large and E small, the trivial solution of the Mathieu equation is stable, see [14, Section 4.80].

• If the amplitude of the activating interval for the energy of residual mode z_i is small, then there is no "visible" activation, see Tables 2 and 3 and use (3.1) to obtain the response in terms of the energy.

4   Different potentials

It is quite natural to wonder whether the results of the previous sections, in particular the numerical results of Section 3, apply to different potentials U, other than (2.3).

If we replace (2.3) with

$$U(y, z_1, z_2) = \frac{\gamma y^2 z_1^2 + \beta y^2 z_2^2 + z_1^2 z_2^2}{2} \quad \gamma, \beta > 0\,,$$

then (2.6) becomes

$$\begin{cases} \ddot{\xi}_1 + \left(\lambda_1^2 + \frac{\gamma x_0^2}{2} + \frac{\gamma x_0^2}{2}\cos(2\mu t)\right)\xi_1 = 0 \\ \ddot{\xi}_2 + \left(\lambda_2^2 + \frac{\beta x_0^2}{2} + \frac{\beta x_0^2}{2}\cos(2\mu t)\right)\xi_2 = 0\,. \end{cases}$$

Whence, we still obtain Mathieu equations of the form (2.7) but with

$$\alpha_1 = \frac{2\lambda_i^2 + \gamma x_0^2}{2\mu^2} \quad \text{and} \quad q_1 = \frac{\gamma x_0^2}{4\mu^2}\,, \quad \alpha_2 = \frac{2\lambda_i^2 + \beta x_0^2}{2\mu^2} \quad \text{and} \quad q_2 = \frac{\beta x_0^2}{4\mu^2}\,.$$

We note that in both the cases there holds $\alpha_i = \frac{\lambda_i^2}{\mu^2} + 2q_i$. Hence, we have different parametrizations of the same parallel lines. In terms of our stability analysis the values of γ and β may be exploited to increase or decrease the energy threshold for the stability of the corresponding equations, see the proof of Theorem 2.3.

More generally, let U be a non-negative, differentiable function with locally Lipschitz derivatives such

that $\nabla U(y,0,0) = (0,0,0)$ for all $y \in \mathbb{R}$. Then, all the above analysis holds and (2.6) becomes

$$\begin{cases} \ddot{\xi}_1 + \left(\lambda_1^2 + U_{z_1 z_1}(x_0 \cos(\mu t), 0, 0)\right) \xi_1 = 0 \\ \ddot{\xi}_2 + \left(\lambda_2^2 + U_{z_2 z_2}(x_0 \cos(\mu t), 0, 0)\right) \xi_2 = 0. \end{cases} \tag{4.1}$$

One may obtain different lines, other than (2.8), for instance by taking non-polynomial potentials U, in which case Hill equations show up instead of the simpler Mathieu equations in (2.7). Then, the stability regions may have strange shapes (see [8]) and it becomes more difficult to determine a precise criterion governing the energy transfer between modes.

Notice that if the potential $U = U(y, z_1, z_2)$ satisfies

$$U_{z_1 z_1}(y, 0, 0) = U_{z_2 z_2}(y, 0, 0) = 0 \qquad \forall y \in \mathbb{R}, \tag{4.2}$$

then the linearized problem (4.1) simply becomes

$$\ddot{\xi}_1 + \lambda_1^2 \xi_1 = 0, \quad \ddot{\xi}_2 + \lambda_2^2 \xi_2 = 0 \tag{4.3}$$

and is therefore independent of y and of its amplitude of oscillation. As an example, consider the potential

$$U(y, z_1, z_2) = \frac{y^4 z_1^4 + y^4 z_2^4 + z_1^4 z_2^4}{4}$$

so that (2.1) becomes

$$\begin{cases} \ddot{y} + \mu^2 y + (z_1^4 + z_2^4)y^3 = 0 & y(0) = x_0, \ \dot{y}(0) = 0 \\ \ddot{z}_1 + \lambda_1^2 z_1 + (y^4 + z_2^4)z_1^3 = 0 & z_1(0) = \varepsilon x_0, \ \dot{z}_1(0) = 0 \\ \ddot{z}_2 + \lambda_2^2 z_2 + (y^4 + z_1^4)z_2^3 = 0 & z_2(0) = \varepsilon x_0, \ \dot{z}_2(0) = 0. \end{cases} \tag{4.4}$$

In this case, the parametric equations (2.8) make no sense and the corresponding (green) lines in Figure 2 are horizontal: this is why we call this case *degenerate*. We have tried some numerical experiments; let us describe some of the results we obtained.

• If $\mu = \lambda_1 = 1$, $\lambda_2 = 2$ and $\varepsilon = 10^{-3}$, the system was extremely unstable. The residual mode z_1 started capturing the energy of y even for small values of x_0. With some fine experiments we could detect instability already for $x_0 = 0.5$, but we suspect the system to be unstable since the very beginning. Completely similar results were obtained for other choices of $\lambda_2 > \lambda_1 = \mu$. And also the case $\lambda_2 = \lambda_1 = \mu$ gave similar response with the addition (of course!) that both z_1 and z_2 captured the energy of y.

• If $\mu = 1$, $\lambda_1 = \sqrt{2}$, $\lambda_2 = 2$, $x_0 = 1$ and $\varepsilon = 0.5$, a large ε compared with Section 3; the reason of this choice is that for smaller ε no interesting phenomenon was evident. We found that the dominating mode y captured some small amount of energy from the residual mode z_2. Therefore, it is *not true* that the energy always moves from the dominating to a residual mode, also the dominating mode can capture the energy and become "more dominating". This seems to be related to the "end of the black bumps" displayed in many plots, see e.g. Figure 1, namely to the interval of time where the residual mode returns the energy to the dominating mode.

• If $\mu = 1$, $\lambda_1 = \sqrt{2}$, $\lambda_2 = 2$ and $\varepsilon = 10^{-3}$, we could see some energy going from y to z_2 only for $x_0 \geq 10$. Therefore, the system turned out to be very stable. We suspect that, again, the ratios λ_i/μ play a major role.

What we have seen in this section suggests that degenerate problems such as (4.4) are either extremely unstable (manifesting instability for very small energies) or extremely stable with instability appearing only for very large energies. This alternative depends on the ratios λ_i/μ. It is also clear that (4.4) cannot remain stable for any energy since (4.3) fails to take into account both the interactions between the residual modes and the perturbations of the periodic solution $y(t) = x_0 \cos(\mu t)$: these are fairly small but for large energies they certainly play some role.

Summarizing, the degenerate problem (4.4), where (4.2) holds, and the corresponding linearized problem (4.3) behave quite differently when compared to (2.4) and a neat pattern as the one described in Section 3 is not available.

5   Mechanical interpretation and structural remedies

In this section we aim to justify from a mechanical point of view the numerical results found in the previous sections. Let us first summarize the main phenomena observed.

(I) As long as the two couples of parameters (q, a) of (2.8) lie in the (white) stability region of the Mathieu diagram, see Figures 4 and 6, the solution $(\bar{y}, 0, 0) = (x_0 \cos(\mu t), 0, 0)$ to system (2.4) is stable, see Definition 2.1.

(II) When a couple (q, a) lies in an instability region and is sufficiently far from the stability region, then the corresponding residual modes become fairly large.

(III) When the couple (q, a) lies in an instability region but is close to the stability region, our numerical results could not detect a neat instability.

The most intriguing result is certainly (III). In order to better understand it, we compared this behavior with the somehow related behavior of the classical linear Mathieu equation

$$\ddot{w} + \Big(a + 2q\cos(2t) \Big) w = 0 \,. \tag{5.1}$$

To obtain two independent solutions, we plotted the two solutions with initial data $(w(0), \dot{w}(0)) \in \{(1, 0); (0, 1)\}$. We analyzed in particular the two first instability regions. From (2.12) we know that (q, a) lies in the first (resp. second) instability region for small enough q if

$$1 - q + O(q^2) < a < 1 + q + O(q^2) \qquad \Big(\text{resp. } 4 - \frac{1}{12}q^2 + O(q^4) < a < 4 + \frac{5}{12}q^2 + O(q^4) \Big).$$

Therefore, we considered couples such as $(q, a) = (q, 1)$ and $(q, a) = (q, 4)$ for $q > 0$ sufficiently small and we could observe the following facts.

(IV) The solutions were always unbounded (thereby confirming instability).

(V) For very small q the solutions became large only after a long interval of time.

(VI) For larger values of q the solutions became large much earlier in time.

(VII) For the same $q > 0$ the instability was more evident when $a = 1$ than when $a = 4$.

The observation (VII) appears strictly related to (II) and (III) and enables us to conclude that

if the couple (q, a) lies in the instability region of the Mathieu diagram, then the instability of the trivial solution of (5.1) increases with the distance of the couple (q, a) from the stability regions.

The model system (2.4) is nonlinear and all its solutions are bounded in view of the energy conservation. Whence, we cannot expect that its solutions start increasing in amplitude as for (5.1). Roughly speaking,

when the residual mode exhibits a tendency to grow up, the energy conservation bounces it back and decreases its amplitude.

We can however expect that the residual modes start growing up earlier in time and wider in amplitude if the parameters are far from the stability region. This is precisely what we saw in our experiments, see Figure 3. In particular, when the parametric lines (2.9) reach and intersect a thin instability region (one of the cusps close to some $a = n^2$ with $n \geq 2$), the parameters are so close to the stability region that the energy inhibits the residual modes to capture a significant amount of energy. From the physical point of view, the instability which occurs when the lines (2.9) cross a thin cusp is irrelevant, both because it has low probability to occur and because, even if it occurs, the residual mode remains fairly small. In turn, from the mechanical point of view, we know that small torsional oscillations are harmless and the bridge would remain safe. Summarizing, we conclude that

when the parametric lines (2.9) cross a thin instability region, only small torsional oscillations appear and the bridge basically remains stable.

From the Mathieu diagram and from the asymptotic expansions of the characteristic curves, see [14, Sections 2.151], we learn that the instability regions become more narrow as $a = n^2$ increases. Since the parametric lines (2.9) take their origin when $a = \lambda_i^2/\mu^2$ (see the right picture in Figure 2), it would be desirable that $\lambda_i \gg \mu$. This gives a structural remedy to improve the torsional stability of a bridge:

the torsional stability of a suspension bridge depends on the ratios between the torsional frequencies and the vertical frequencies; the larger they are, more stable is the bridge.

Therefore, our results suggest that bridges should be designed in such a way that these ratios are very large.

References

[1] M. ABRAMOWITZ AND I.A. STEGUN, *Handbook of Mathematical Functions with Formulas, Graphs, and Mathematical Tables*, Dover, New York, 1972.

[2] O.H. AMMANN, T. VON KÁRMÁN AND G.B. WOODRUFF, *The failure of the Tacoma Narrows Bridge*, Federal Works Agency, Washington D.C., 1941.

[3] G. ARIOLI AND F. GAZZOLA, *A new mathematical explanation of what triggered the catastrophic torsional mode of the Tacoma Narrows Bridge collapse*, to appear in Appl. Math. Modelling

[4] E. BERCHIO AND F. GAZZOLA, *A qualitative explanation of the origin of torsional instability in suspension bridges*, arXiv:1404.7351

[5] E. BERCHIO AND F. GAZZOLA, *The role of aerodynamic forces in a mathematical model for suspension bridges*, arXiv:1409.1769

[6] F. BLEICH, *Dynamic instability of truss-stiffened suspension bridges under wind action*, Proceedings ASCE, 74 (1948), pp. 1269-1314.

[7] F. BLEICH, C.B. MCCULLOUGH, R. ROSECRANS AND G.S. VINCENT, *The mathematical theory of vibration in suspension bridges*, U.S. Dept. of Commerce, Bureau of Public Roads, Washington D.C., 1950.

[8] H. BROER AND M. LEVI, *Geometrical aspects of stability theory for Hill's equations*, Arch. Rational Mech. Anal., 131 (1995), pp. 225-240.

[9] M. COMO, S. DEL FERRARO AND A. GRIMALDI, *A parametric analysis of the flutter instability for long span suspension bridges*, Wind and Structures, 8 (2005), pp. 1-12.

[10] G.W. HILL, *On the part of the motion of the lunar perigee which is a function of the mean motions of the sun and the moon*, Acta Math., 8 (1886), pp. 1-36.

[11] W. LACARBONARA, *Nonlinear structural mechanics*, Springer, 2013.

[12] E. MATHIEU, *Mémoire sur le mouvement vibratoire d'une membrane de forme elliptique*, J. Math. Pure Appl., 13 (1868), pp. 137-203.

[13] P.J. McKenna and C.Ó Tuama, *Large torsional oscillations in suspension bridges visited again: vertical forcing creates torsional response*, Amer. Math. Monthly, 108 (2001), pp. 738-745.

[14] N.W. McLachlan, *Theory and application of Mathieu functions*, Dover Publications, Inc. New York, 1964.

[15] B.G. Pittel and V.A. Yakubovich, *A mathematical analysis of the stability of suspension bridges based on the example of the Tacoma Bridge (Russian)*, Vestnik Leningrad Univ., 24 (1969), pp. 80-91.

[16] H. Poincaré, *Introduction to the collected mathematical works of George William Hill*, Carnegie Institution of Washington, Vol. I, 1905, pp.vii-xviii.

[17] H. Poincaré, *Les méthodes nouvelles de la mécanique céleste*, Dover Publications, New York, 1957.

[18] Y. Rocard, *Dynamic instability: automobiles, aircraft, suspension bridges*, Crosby Lockwood, London, 1957.

[19] R.H. Scanlan and J.J. Tomko, *Airfoil and bridge deck flutter derivatives*, J. Eng. Mech., 97 (1971), pp. 1717-1737.

[20] R. Scott, *In the wake of Tacoma. Suspension bridges and the quest for aerodynamic stability*, ASCE Press, 2001.

[21] D.B. Steinman, *Design of bridges against wind: IV, Aerodynamic instability - prevention and cure*, Civil Engineers ASCE, 1946, pp. 20-23.

[22] F. Verhulst, *Perturbation analysis of parametric resonance*, In: Encyclopedia of Complexity and Systems Science, Springer, 2009, pp. 6625-6639.